Kinetics and Catalysis, Vol. 45, No. 1, 2004, pp. 1–9. Translated from Kinetika i Kataliz, Vol. 45, No. 1, 2004, pp. 3–11.

Transition of Flame Propagation from Isothermal to Thermal Regimes in Chain Processes with Nonlinear Chain Branching

N. M. Rubtsov*, V. D. Kotelkin, and V. P. Karpov*****

** Institute of Structural Macrokinetics and Problems of Materials Science, Russian Academy of Sciences, Chernogolovka, Moscow oblast, 142432 Russia*

*** Faculty of Mechanics and Mathematics, Moscow State University, Moscow, 119992 Russia*

**** Semenov Institute of Chemical Physics, Russian Academy of Sciences, Moscow, 119991 Russia*

Received December 4, 2002

Abstract—The transition of an isothermal flame to a thermal combustion regime is considered experimentally and theoretically for the thermal decomposition of nitrogen trichloride. Experimental data on the transition of a thermal regime of flame propagation to a chain-thermal explosion are presented for dichlorosilane oxidation. One of the ways for the development of the chain-thermal explosion is shown to be the appearance of a local center of intense combustion in the thermal flame front.

INTRODUCTION

Two mechanisms of propagation of subsonic flames, *viz*., isothermal and thermal, are known in the combustion theory [1]. Let us consider the specific features of flame propagation in a branched chain process. The structure of the ignition regime for the branched chain process in the pressure–temperature coordinates is presented in Fig. 1 [2–4]. The rate of isothermal flames (region **I**) is determined by the diffusion of active centers of the branched chain process to the unreacted mixture, and the branched chain mechanism should include nonlinear branching (in this reaction, the number of free valences increases, for example, when the active centers interact with each other [2, 3]). Unlike isothermal flames, the specific features of thermal flames are determined by a heat release in the front of the branched chain process. The very strong, non-Arrhenius [4–6] temperature dependence of the rate of the branched chain process is the feedback factor providing the appearance of a stationary combustion front. These flames have extensively been studied for the branched chain processes containing only linear (with respect to active centers) branching reactions (for example, [7, 8]). The self-ignition region of linear branched chain processes **II** includes the region of chain-thermal explosion **IIc**. The chain-thermal explosion implies the regime of chain combustion including both the chain collapse and self-heating, as well as the collapse character of heat accumulation in the system when the rate of heat release q^+ is higher than the rate of heat removal q^-; $q^+ - q^- = \Delta q > 0$, and $d\Delta q/dT > 0$ [4, 5].

The stationary flame propagation in linear branched chain processes is excluded in region **IIa** near the lower self-ignition limit because $q \approx 0$, that is, the cited feedback factor is absent. At $\Delta q > 0$ (region **IIb**), the stationary wave of thermal combustion can appear (thin arrows in Fig. 1). This regime can be named more specifically the chain-thermal regime because the competition of chain branching and termination is the determining factor for the flame propagation [4]. The combustion flame in the chain-thermal explosion region (**IIc**) should possess different properties. In fact, according to data presented in [4], the concentration limits of the chain-thermal explosion for hydrogen–oxygen mixtures are close to the detonation limits of these mixtures. This means that one has to expect the

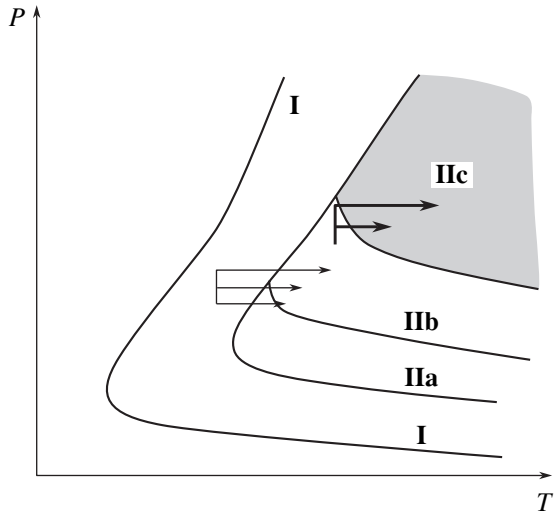

Fig. 1. Scheme of the ignition regions in the branched chain process: (**I**) isothermal flame propagation; (**IIa**) isothermal self-ignition; (**IIb**) thermal flame propagation; and (**IIc**) chain-thermal explosion. Transition of the isothermal regime of flame propagation to the thermal regime is shown by thin arrows; transition of the thermal flame propagation to the chain-thermal explosion is shown by bold arrows. The arrow lengths correspond to the self-heating value.

0023-1584/04/4501-0001 © 2004 MAIK "Nauka / Interperiodica"

appearance of transition combustion regimes between the thermal regime of flame propagation and the chain-thermal explosion region. This transition regime is characterized by spatial heterogeneity. This was indicated, for example, in [9] for monosilane oxidation studied by the separate photometric method and in [10].

In this work, we consider the transition of the flame propagation regime from region **I** to **IIb** (thin arrows in Fig. 1), which is only possible in branched chain processes with nonlinear branching, and some specific features of the transition of the thermal flame propagation regime to the chain-thermal explosion region **IIc** (solid arrows in Fig. 1). These aspects have not been discussed earlier.

Isothermal flames have been observed in dilute mixtures of CS_2 with O_2 [2, 3], for the thermal decomposition of nitrogen trichloride (NCl_3) [11], fluorination of difluoromethane [12], and oxidation of monosilane and dichlorosilane [13, 14]. Since these flames appear at very low concentrations of fuel (~0.03% [2, 3]), researchers are interested in them because of problems of explosion safety: NCl_3 is formed in the industrial production of chlorine [15], and silanes are widely used in microelectronics [16]. Therefore, it is important to establish regularities of the flame propagation in branched chain processes, including nonlinear branching. The thermal decomposition of NCl_3 is a branched chain process of decomposition of an individual substance in the gas phase at room temperature. Since the kinetic mechanism of NCl_3 decomposition is known [11, 17–19], the branched chain process is convenient for considering the transition of the isothermal flame to the thermal regime. Unlike the branched chain decomposition of NCl_3 whose energy is consumed predominantly for the formation of atoms and radicals and whose heat release is comparatively low [17], the branched chain oxidation of dichlorosilane is strongly exothermic (the heat of dichlorosilane combustion is ~170 kcal/mol [20]) and, hence, this process is convenient for considering the transition of the thermal flame propagation to the chain-thermal explosion.

The purpose of this work is to establish regularities of the transition of the isothermal flame to the thermal regime for the branched chain decomposition of NCl_3 and to reveal the spatial features of the transition of the thermal regime of flame propagation to the chain-thermal explosion for the branched chain oxidation of dichlorosilane.

EXPERIMENTAL

Experiments with NCL_3 were carried out under static conditions at P = 2–100 Torr, T = 293 K, and $[NCl_3]$ = 0.11–4.00% in a glass vacuum setup described in [11]. A quartz tube, 80 cm long and 4 cm in diameter, was used as a reactor. The procedure of measuring the flame rates has been described in [21]. The reactor surface was covered by magnesium oxide, which provided the diffusion region of chain termination at room temperature [11, 17]. In kinetic measurements, the pressure was detected using a diaphragm pressure gauge, whose lower measurement limit was 5×10^{-3} Torr. The concentration of NCl_3 was determined according to the total stoichiometry of the reaction $2NCl_3 \longrightarrow N_2 + 3Cl_2$ [18]. Liquid NCl_3 was synthesized and its mixtures with He were prepared according to procedures described in [17]. Before each experiment, the reactor was evacuated to 4×10^{-4} Torr (measurements were carried out using a VIT-3 vacuum gauge). The spark-initiated ignition of the preliminarily prepared mixtures of 5% dichlorosilane with dioxygen was studied at an initial temperature of 300 K and pressures of 300–450 Torr. The reactor was a metallic cylinder with a diameter and a height of 10 cm equipped with optical windows and electric and gas inlets. The optical system was a schlieren setup. The experimental procedure, including recording the images of the optical heterogeneity, has been described in [22]. The reactor was evacuated to 10^{-2} Torr using a 2NVR-5D roughing-down pump, and the pressure was detected by a standard vacuum gauge. Dichlorosilane (98% [23]), He, O_2, and SF_6 (reagent grade) were used.

RESULTS AND DISCUSSION

It has previously been shown [11] that the pressure interval in which the isothermal flame is observed (Fig. 2a) expands with an increase in the NCl_3 concentration, and the upper limit of flame propagation is not detected above a certain NCl_3 concentration in He (Fig. 2b, points). This indicates a substantial increase in the role of self-heating. Let us qualitatively interpret the regularities of the nonthermal flame propagation observed for the known one-step mechanism of NCl_3 decomposition and describe the calculation algorithm.

The kinetic mechanism of the branched chain decomposition of NCl_3 can be presented as follows [11, 17–19].

$$(0)\ NCl_3 \longrightarrow NCl_2 + Cl,$$

$k_0 = 10^{-3}$–10^{-5} s^{-1} [24], chain initiation;

$$(1)\ Cl + NCl_3 \longrightarrow NCl_2 + Cl_2 + Q_1,$$

$k_1 = 1.6 \times 10^{-12}$ cm^3/s [24], chain propagation;

$$(2)\ NCl_2 + NCl_3 \longrightarrow N_2 + Cl_2 + 3Cl + Q_2,$$

$k_2 = 3.4 \times 10^{-11}\exp(-\varepsilon_1/T)$ cm^3/s, $\varepsilon_1 = 3050/R$ deg (E_a in cal/mol) [25–27], linear branching;

$$(3)\ NCl_2 + NCl_2 \longrightarrow N_2 + Cl_2(^3\Pi_{ou}^+) - 2Cl,$$

$k_3 = 6.0 \times 10^{-13}$ cm^3/s [28, 29], nonlinear chain termination;

$$(4)\ Cl_2(^3\Pi_{ou}^+) \longrightarrow 2Cl,$$

$k_4 = 4.8 \times 10^2$ s^{-1} [18, 30];

(5) $Cl_2(^3\Pi_{ou}^+) + Cl \longrightarrow Cl_2(^1\Sigma_g^-) + Cl$,

$k_5 = 1.6 \times 10^{-10}$ cm^3/s [31, 32],

nonlinear chain termination;

(6) $NCl_2 \longrightarrow$ wall, k_6, heterogeneous termination in diffusion region;

(7) $Cl \longrightarrow$ wall, k_7, heterogeneous termination in diffusion region;

(8) $Cl_2(^3\Pi_{ou}^+) + M \longrightarrow Cl(^1\Sigma_g^-) + M$,

$k_8 = 8 \times 10^{-13}$–10^{-13} cm^3/s [31], deactivation.

Let us consider the specific features of the mechanism of NCl_3 decomposition. Since heterogeneous chain termination was considered in the diffusion region [8], the k_7 and k_8 rate constants were calculated using the formula $k = 23.2D_i/(d^2P)$ [3], where d is the diameter of the reactor, and P is the total pressure. The D_i values in He (cm^2/s, 293 K, 760 Torr) were taken from [26, 32]

Cl	NCl_2	$Cl_2(^3\Pi_{ou}^+)$	NCl_3	He
0.73	0.44	0.55	0.41	1.62

Steps (0)–(8) and kinetic constants are identical to those used for the calculation in [18, 19]. In our calculation, the thermal effect Q_1 was either 0 or 17 kcal/mol, and Q_2 was taken equal to 34 kcal/mol. These values correspond to the published data on the energies of the N–Cl bonds in the NCl_3 molecule [32]. Taking into account step (8), we can explain the presence of the upper limit of flame propagation [19]. The k_8 value providing the agreement between the experimental and calculated data [19] effectively takes into account the contribution of the termolecular chain termination at the upper limit of the isothermal flame propagation, which is not included in the scheme and, therefore, is the upper boundary of the rate constant of step (8).

A lack of experimental data prevent us from introducing the termolecular chain termination in the reaction mechanism. The upper self-ignition limit for NCl_3 ($\mathbf{P}_2$) was experimentally observed in [25, 33]. Therefore, at least one more chain termination reaction occurs along with termination (8) because the decay of only $Cl_2(^3\Pi_{ou}^+)$ in the step of linear branching (2) cannot provide the upper self-ignition limit. In fact, if even two Cl_2 molecules appear in step (2) ($^3\Pi_{ou}^+$) and are deactivated, no termination occurs because one chlorine atom remains. Thus, step (2) remains as the chain termination reaction. Reactions of the type $Cl + NCl_3 + M \longrightarrow$ termination and $NCl_2 + NCl_3 + M \longrightarrow$ termination are expected. At the same time, possible products of these reactions (NCl_4, N_2Cl_3, or N_2Cl_5), which should be chemically unreactive, were not observed experimentally. However, note that $\mathbf{P}_2$ for the thermal decomposition of NCl_3 depends on the chemical nature of the reactor coating: for experiments on the nonthermal flame propagation above magnesium oxide, the $\mathbf{P}_2$ values in the P–T coordinates are almost perpendicular to the abscissa (temperature), which implies the practical absence of $\mathbf{P}_2$, whereas for the KF coating the temperature plot is much less sharp [25]. The practical absence of $\mathbf{P}_2$ in experiments above the magnesium oxide surface indicates that some factor compensates for the homogeneous termolecular termination. This allows us to consider the chain termination reactions in the bulk for NCl_3 decomposition above MgO to be compensated and ignored in calculations. This was made in [19] and in the present work.

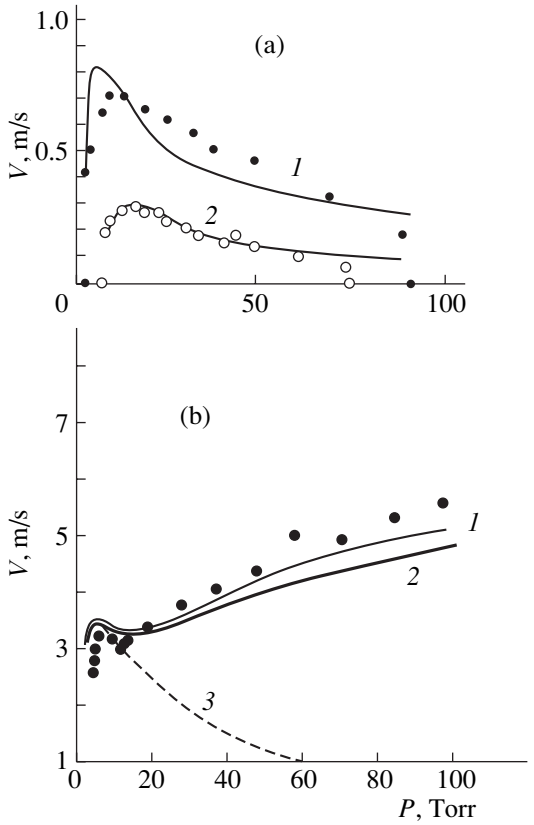

Fig. 2. Plots of the flame propagation vs. total pressure in NCl_3 mixtures with He: (a) nonthermal flame at (*1*) 0.38% and (*2*) 0.11% NCl_3 in He, points are experimental, and curves are calculations [19]; (b) thermal flame, 4% NCl_3 with He; points are experimental, curves are calculations at (*1*) Q_1 = 17 kcal/mol, Q_2 = 34 kcal/mol (one-dimensional problem) [19]; (2) Q_1 = 17 kcal/mol, Q_2 = 34 kcal/mol (two-dimensional problem); and (*3*) Q_1 = 0, Q_2 = 34 kcal/mol (one-dimensional problem).

It has been shown in [19] that the results of numerical simulation of the isothermal flame propagation in NCl_3 mixtures with He, CO_2, and Cl_2 for steps (0)–(8)

agree with the experimental data in the pressure interval from the lower to upper limits. As shown in [19, 29], the rate of linear chain branching is negligible in the region of isothermal flame propagation. At the same time, an increase in the rate of this reaction and, correspondingly, an increase in the heat release with an increase in the NCl_3 content can result in the transition of the isothermal regime of flame propagation to the thermal regime.

In order to reveal the specific features of the qualitative calculation performed, let us consider the two-dimensional problem and choose the characteristic scales: $t_0 = 1/(k_1[NCl_3]_0)$, $x_0 = (D_3/k_1[NCl_3]_0)^{1/2}$, and $U_0 = x_0/t_0 = (D_3k_1[NCl_3]_0)^{1/2}$, where t_0, x_0, and U_0 are the scales of time, lengths, and rate, respectively; D_3 is the diffusion coefficient of NCl_3. Let us introduce dimensionless variables $\tau = t/t_0$, $\xi = x/x_0$, $\eta = y/y_0$ (y is the second dimension of the two-dimensional problem), $\varpi = U/U_0$, $Y_i = [A_i]/[NCl_3]_0$ ($[A_i]$ is the concentration of the ith component), and $\delta_i = D_i/D_3$ (D_i is the diffusion coefficient of the ith component). We obtain $\tau = k_1[NCl_3]_0t$, $Y_0 = [Cl]/[NCl_3]_0$, $Y_1 = [Cl_2(^3\Pi_{ou}^+)]/[NCl_3]_0$, $Y_2 = [NCl_2]/[NCl_3]_0$, $Y_3 = [NCl_3]/[NCl_3]_0$, $\beta = k_2/k_1$, $\phi = k_3/k_1$, $\gamma = k_7/(k_1[NCl_3]_0)$, $\lambda = k_4/(k_1[NCl_3]_0)$, $\zeta = k_6/(k_1[NCl_3]_0)$, $\mu = k_6/k_1$, and $\chi = k_8/(k_1[NCl_3]_0)$. The total pressure (Torr) is designated by P, that is, $[NCl_3]_0 = sP$, where s is the molar fraction of NCl_3 in the initial mixture, and the time (s) is designated by t. The dimensionless rate and coordinates of the front of the propagating flame were determined through the diffusion coefficients of $NCl_3(D_3)$: $\varpi = U/(D_3k_1[NCl_3]_0)^{1/2}$, $\xi = x/(D_3/k_1[NCl_3]_0)^{1/2}$, and $\eta = y/(D_3/k_1[NCl_3]_0)^{1/2}$, where U, x, and y are the corresponding dimensional values. The dimensionless diffusion coefficients (D_i/D_3, $i = 0$–2) δ_0, δ_1, and δ_2 in He are referred to the chlorine atoms $Cl_2(^3\Pi_{ou}^+)$ and $NCl_2^{\bullet}$ radicals, respectively. The stationary propagation of the chemical reaction wave was considered ignoring the chain initiation rate [34]. The system of two-dimensional diffusion kinetic equations for the reaction mechanism presented has the following form (the one-dimensional problem was considered in [19]):

$$\begin{aligned}
\partial Y_0/\partial\tau &= \delta_0(\partial^2Y_0/\partial\xi^2 + \partial^2Y_0/\partial\eta^2) + 2\phi(Y_2)^2 \\
&+ 3Y_2Y_3\beta\exp(-3050/T) + 2\lambda Y_1 - Y_0Y_3 - \gamma Y_0, \\
\partial Y_1/\partial\tau &= \delta_1(\partial^2Y_1/\partial\xi^2 + \partial^2Y_1/\partial\eta^2) \\
&+ 2\phi(Y_2)^2 - \lambda Y_1 - \chi P Y_2, \\
\partial Y_2/\partial\tau &= \delta_2(\partial^2Y_2/\partial\xi^2 + \partial^2Y_2/\partial\eta^2) - 2\phi(Y_2)^2 \\
&- \xi Y_2 - Y_2Y_3\beta\exp(-3050/T), \\
\partial Y_3/\partial\tau &= (\partial^2Y_3/\partial\xi^2 + \partial^2Y_3/\partial\eta^2) \\
&- Y_0Y_3 - Y_2Y_3\beta\exp(-3050/T), \\
\partial T/\partial\tau &= \delta_4(\partial^2T/\partial\xi^2 + \partial^2T/\partial\eta^2) \\
&+ s\beta(k_2Y_2Y_3\exp(-3050/T)Q_1 + Y_0Y_3Q_2)/(c_p\rho) = \Delta q.
\end{aligned} \tag{1}$$

The rate of heat release in the reaction chain unit is described by the latter equation in system (1), where c_p is the thermal capacity at a constant pressure (1.25 cal g^{-1} deg^{-1} for He [35]), T is temperature (K), $\delta_4 = D_{(He–He)}/(D_3c_p\rho)$, and ρ is the density of He (g/cm^3) [35]. The solutions to system (1) satisfy the following boundary conditions for the flame propagation from right to left:

$$\begin{aligned}
&Y_0(\xi, \eta), Y_1(\xi, \eta), Y_2(\xi, \eta), T(\xi, \eta) \longrightarrow 0, \\
&\xi \longrightarrow \pm\infty; \\
&Y_3(\xi, \eta) \longrightarrow 1, \quad \xi \longrightarrow -\infty; \\
&Y_3(\xi, \eta) \longrightarrow 0, \quad \xi \longrightarrow +\infty; \\
&Y_0(\xi, I) = 0, \quad (\partial Y_1(\xi, \eta)/\partial\eta)_i = 0, \\
&Y_2(\xi, I) = 0; \quad (\partial Y_3(\xi, \eta)/\partial\eta)_i = 0; \\
&T(\xi, I) = \text{const} \quad \text{or} \\
&-\lambda(\partial T(\xi, \eta)/\partial\eta)_i = \alpha(T - T_0),
\end{aligned} \tag{2}$$

where I is the transversal diameter of the reactor, the symmetry conditions are specified in the axis, and α is the thermal conductivity coefficient, which was estimated from the correlation $\alpha = \Delta\Lambda e/(Lr^2)$ (L is the ratio of the surface area to the volume (cm^{-1}), r is the radius of the reactor (cm), $e = 2.718$, Δ is the critical parameter (2.0) [1], and $\Lambda = D_{(He–He)}$ is the thermal conductivity coefficient for dilute mixtures).

It has been shown that the results of calculations do not change qualitatively when the boundary conditions with respect to T of the first or third order are used. Therefore, the calculations with the first-order boundary condition are presented below. The representation of the Laplacian in the cylindrical coordinates does not result in qualitative changes in simulations either. Set (1) of equations was numerically integrated. The calculation details are presented in Appendix.

The upper limit of the isothermal flame propagation at $[NCl_3] = 4\%$ is not observed in either experiment or simulation. It can easily be seen by comparing data in Figs. 2a and 2b that two solutions corresponding to the thermal and isothermal flames are valid at the same total pressure (in the given case >35 Torr) and different concentrations of NCl_3. Furthermore, at $[NCl_3] = 0.38\%$ the thermal flame is not observed in either calculation or experiment. This implies that the possibility of transition to the thermal regime of flame propagation is determined by the initial concentration of NCl_3 and has the critical character with respect to pressure (Fig. 2b).

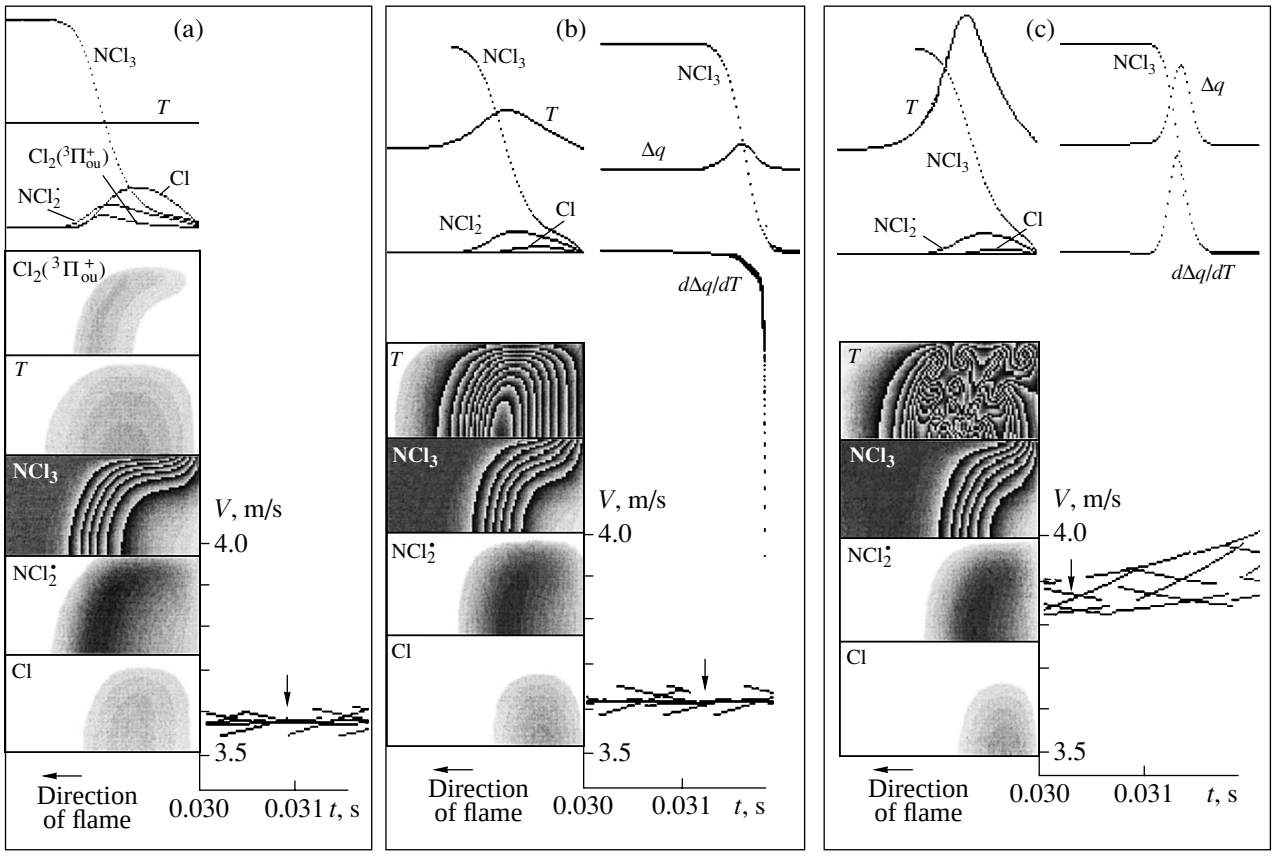

Fig. 3. Distributions of the components and flame rates for different regimes of combustion wave propagation (T_0 = 300 K, two-dimensional problem): (a) P = 5 Torr, 4% NCl_3 in He, isothermal flame propagation; (b) P = 35 Torr, 4% NCl_3 in He, thermal flame propagation; and (c) P = 5 Torr, 14% NCl_3 in He, c_p = 0.125 cal g^{-1} deg^{-1}, transition to chain-thermal explosion. (For clarification of the figure, see text.)

It can be seen from data in Fig. 2b that the isothermal flame occurs at low pressures, and then with the pressure increase the transition to the thermal regime occurs at $P \sim 20$ Torr. This transition pressure corresponds to a pressure value at which the experimental plot of the flame rate vs. P has a break and the calculated curves presented in Fig. 2b diverge. The flame rates calculated using the one-dimensional [19] and two-dimensional models are very close (Fig. 2b, curve *3*). Note that taking into account the heat release only in the step of linear chain branching (2) ($Q_1 = 0$, Q_2 = 34 kcal/mol) does not result in the transition to the thermal regime at pressures below 100 Torr (Fig. 2b). Therefore, the heat release in step (1) was also taken into account. However, note that the very broad confidence intervals for the parameters determining the heat release (Q_1, Q_2, α, and ε_1) make it only possible to speculate on the qualitative agreement between the experimental and simulated data. We did not attempt to attain the coincidence of the simulated and experimental values of the rate and limits of flame propagation by the variation of the k_i constants. This fitting is not valuable because the simulation makes use of many parameters.

Analysis of the two-dimensional problem resulting in the qualitatively valid results for the transition of the isothermal regime of flame propagation to the thermal regime was also applied for the consideration of the stability boundary of the thermal regime of flame propagation. We studied the spatial features of the appearance of instabilities under the condition $d\Delta q/dT > 0$ along with the condition $\Delta q > 0$, which is already fulfilled in the region of thermal flame propagation **IIb**. The results of simulations are presented in Fig. 3. The left bottom corner of each fragment (a–c) contains the distributions of the temperature and concentrations of the NCl_3 molecules, $NCl_2^{\bullet}$ radicals, and chlorine atoms over the reactor. The simulated $[Cl_2(^3\Pi_{ou}^+)]$ values in the thermal flame front are ~10 times lower than those in the nonthermal flame front. Therefore, the two-dimensional distributions $Cl_2(^3\Pi_{ou}^+)$ were not simulated under the conditions presented in Figs. 3b, 3c and 4b, 4c, 4d. The authors of [36] have found that an increase in the total pressure increases the chemiluminescence intensity of $Cl_2(^3\Pi_{ou}^+)$ in the 2–5 Torr pressure interval (depending on the NCl_3 concentration), and then the chemilumines-

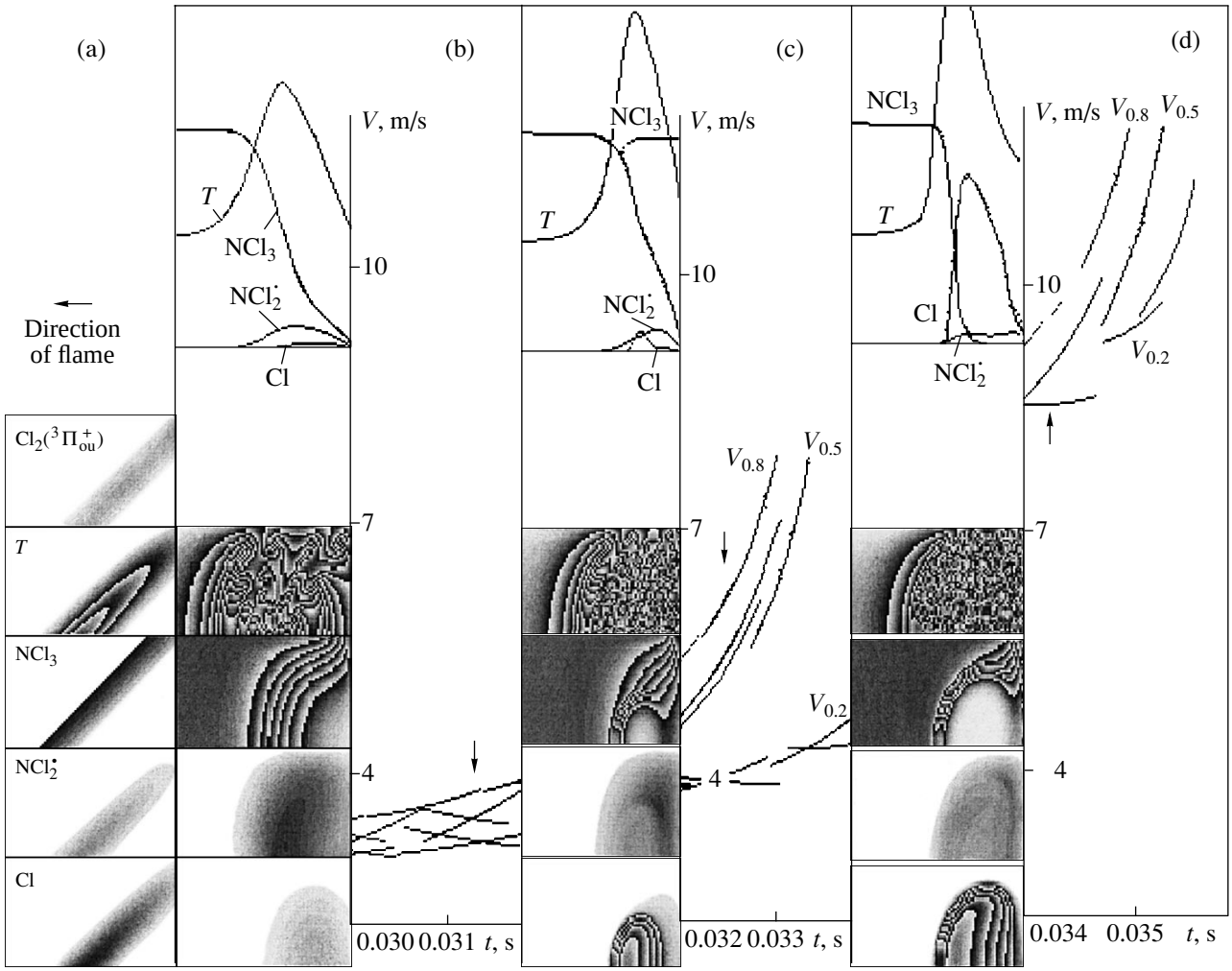

Fig. 4. (a) Initial distributions and (b, c, d) distributions of the components and flame rates on going from the thermal flame propagation to the chain-thermal explosion. Vertical arrows indicate the moments corresponding to the distributions presented in the figure. Dotted lines in the plot of V vs. t reflect the specificity of calculation related to the relatively large counting increment for obtaining a reasonable counting time. (For clarification to $V_{0.2}$, $V_{0.5}$, and $V_{0.8}$, see Appendix.)

cence intensity decreases sharply. This fact agrees qualitatively with the calculated result obtained, as well as the maximum concentrations of the $NCl_2^{\bullet}$ radicals [21] and Cl atoms [25].

The lines in the two-dimensional distributions correspond to constant concentrations. The distributions between the wall and axis of the reactor were determined because the problem is centrally symmetric. Thus, in each of four two-dimensional distributions (five for Fig. 3a) the top of the "frame" is the reactor wall and the bottom of the frame is the reactor axis. The one-dimensional distributions of the components over the reactor axis are presented in the left top corner. The right part of each fragment contains data for the establishment of the stationary rate value (Fig. 3c) or the rate corresponding to the established stationary regime (Figs. 3a, 3b). The vertical arrows indicate the time at which the distributions were detected. The right top corners in Figs. 3b and 3c show changes in the NCl_3 concentration and the Δq and $d\Delta q/dT$ values in the flame front in the one-dimensional form along the reactor axis.

Figure 3b shows that $\Delta q > 0$ in the established regime of thermal combustion, and $d\Delta q/dT < 0$. However, when the condition $d\Delta q/dT > 0$ is fulfilled, as can be seen from the data in Fig. 3c, the thermal flame loses its stability, and its rate begins to increase. This condition, as shown in [4], corresponds to the transition of the thermal ignition of combustion to the chain-thermal explosion regime. Region **IIc** corresponds to this regime in Fig. 1. Note that the transition of the thermal flame propagation to the regime where $d\Delta q/dT > 0$ cannot be obtained at the values of the parameters of system (1) for NCl_3 decomposition. This qualitative result agrees with the data in [15], which show that NCl_3 mixtures in He in a wide interval of NCl_3 concentrations cannot detonate. However, with a tenfold decrease in

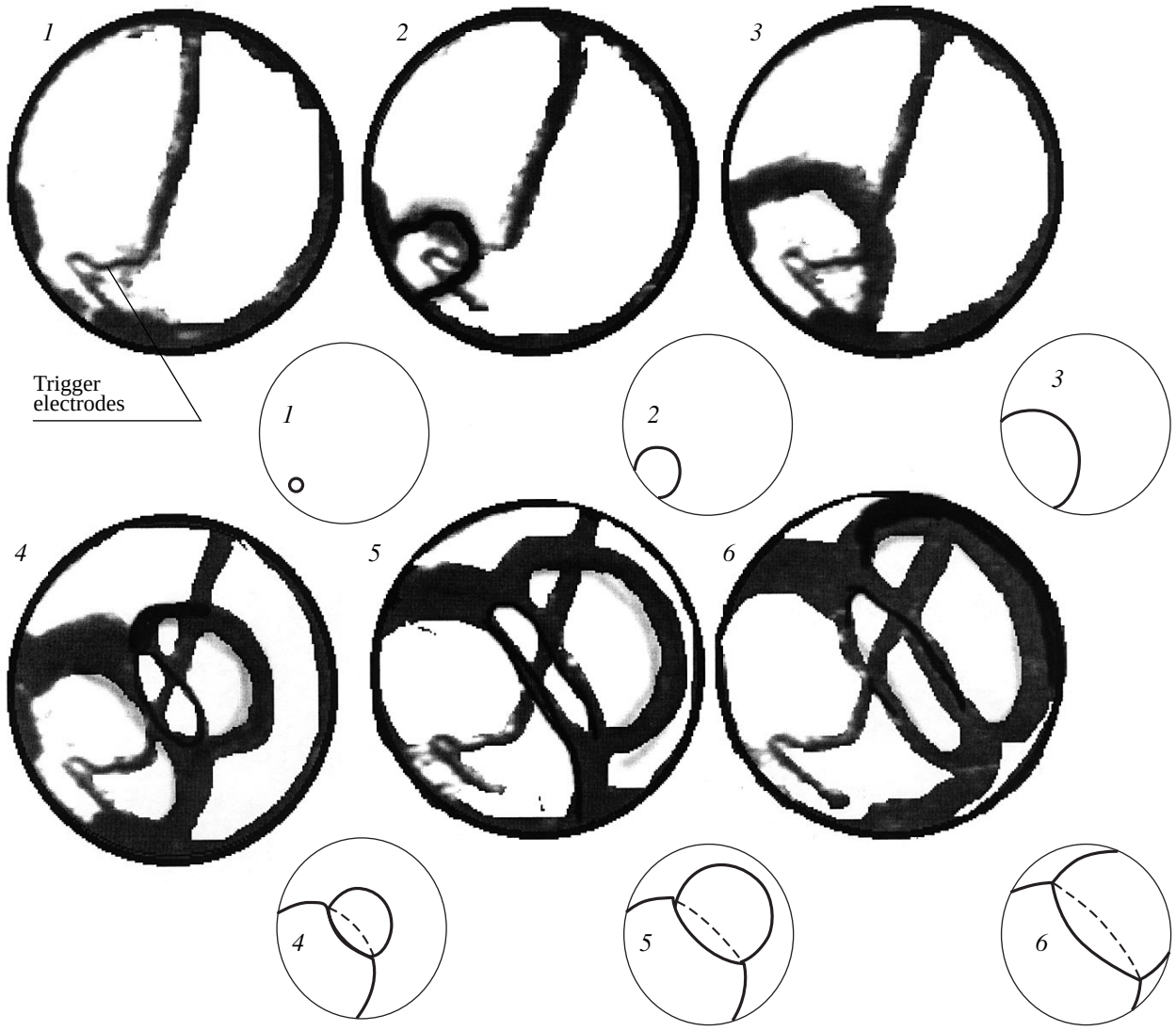

Fig. 5. Development of the initiated ignition of a mixture of 5% dichlorosilane with O_2. Interval between frames is 10^{-3} s, P = 450 Torr, T_0 = 300 K.

the thermal capacity of the system or an increase in the thermal effect of the branched chain process to 100 kcal/mol, the transition shown in Fig. 3c is already observed in simulations. The oxidation of dichlorosilane with oxygen is characterized by these values of parameters. The detailed mechanism of dichlorosilane oxidation is not found. Note that dichlorosilane oxidation is a branched chain process with nonlinear branching [14] and, hence, this reaction should manifest kinetic features similar to those of NCl_3 decomposition.

The simulated changes in the distribution of the components under the chain-thermal explosion conditions are shown in Figs. 4c, 4d, and 4e. The initial conditions (Fig. 4a) were specified in such a way that the time of achievement of the stationary regime would be minimum. The data in Fig. 4c show that the development of the chain-thermal explosion is accompanied by the appearance of the intense combustion center in the front of the stationary thermal flame. Evidently, Figs. 4b and 4c have real physical sense because further transition to the chain-thermal explosion and establishment of the stationary rate of this process require taking into account the equations of gas dynamics and temperature dependences of the thermal capacity and thermal effects of elementary reactions [4].

Experimental data on the detection of this transition regime are presented below for dichlorosilane combustion. Note that, since the detailed mechanism of dichlorosilane oxidation is not found, the results obtained only qualitatively indicate that transitions regimes of combustion wave propagation can occur when the sign at $d\Delta q/dT$ changes. The well reproduced images of the optical heterogeneity of the initiated ignition of the 5% dichlorosilane + O_2 mixture at 450 Torr are presented in

Fig. 5. Initiation was carried out in the left bottom part of the reactor (both trigger electrodes are seen in all frames). The center of intense combustion appears in the flame front 3 ms after initiation (Fig. 5, frame 4), and the flame starts to accelerate. As can be seen from Fig. 5, the thermal flame passes through half a volume of the reactor within ~5 ms, and the center is passed during 1.5 ms. Thus, the center is propagated with a visible rate ~3 times higher than the visible rate of the thermal flame. This estimate is very rough because the propagating flame near the walls is already "tightened" by the unburned gas and is retarded. The role of the Mache effect in the formation of this combustion center is insignificant because the instability is formed at the moment when the flame front is still far from the wall toward which it is propagated. Therefore, the unreacted gas is not heated due to the adiabatic compression. We believe that the transition of the thermal flame to the chain-thermal combustion is experimentally detected in Fig. 5 (frames *4–6*). The formation of the unstable state has a critical character because no instability is observed either in the presence of the weak inhibitor SF_6 (2%) [37] or with a decrease in the total pressure by ~5%: only the uniformly propagating thermal flame is detected.

CONCLUSIONS

Thus, the regularities of the transition of the isothermal flame to the thermal combustion regime were established for the thermal decomposition of nitrogen trichloride using the two-dimensional kinetic model on the basis of the detailed mechanism of the process. Experimental data on the transition of the thermal regime of flame propagation to the chain-thermal explosion were presented for dichlorosilane oxidation. It was experimentally and theoretically shown that one of the ways for development of the chain-thermal explosion can be the appearance of a local center of intense combustion in the thermal flame front.

ACKNOWLEDGMENTS

This work was supported by the Russian Foundation for Basic Research (project nos. 00-03-32979a and 02-03-32993a).

REFERENCES

1. Frank-Kamenetskii, D.A., *Diffuziya i teploperedacha v khimicheskoi kinetike* (Diffusion and Heat Transfer in Chemical Kinetics), Moscow: Nauka, 1967.
2. Voronkov, V.G. and Semenov, N.N., *Zh. Fiz. Khim.*, 1939, vol. 13, p. 1695.
3. Semenov, N.N., *O nekotorykh problemakh khimicheskoi kinetiki i reaktsionnoi sposobnosti* (On Some Problems of Chemical Kinetics and Reactivity), Moscow: Nauka, 1968.
4. Azatyan, V.V., Bolod'yan, I.A., Shebeko, Yu.M., and Kopylov, S.M., *Fiz. Goreniya Vzryva*, 2001, vol. 37, no. 5, p. 12.
5. Azatyan, V.V. and Merzhanov, A.G., *Khimicheskaya fizika na poroge XXI veka* (Chemical Physics on the Threshold of the 21st Century), Sergeeva, G.B. and Shilova, A.E., Eds., Moscow: Nauka, 1996, p. 74.
6. Azatyan, V.V. and Shavard, A.A., *Izv. Akad. Nauk SSSR, Ser. Khim.*, 1977, no. 11, p. 2460.
7. Zel'dovich, Ya.B., Barenblatt, G.I., Librovich, V.B., and Makhviladze, G.M., *Matematicheskaya teoriya goreniya i vzryva* (Mathematical Theory of Combustion and Explosion), Moscow: Nauka, 1980.
8. Lewis, B. and von Elbe, G., *Combustion, Explosions, and Flame in Gases*, New York, 1987.
9. Azatyan, V.V. and Aivazyan, R.G., *Kinet. Katal.*, 1986, vol. 27, no. 5, p. 1086.
10. Azatyan, V.V., Vartanyan, A.A., Kalkanov, V.A., and Shavard, A.A., *Khim. Fiz.*, 1989, vol. 8, p. 1290.
11. Azatyan, V.V., Borodulin, R.R., and Rubtsov, N.M., *Fiz. Goreniya Vzryva*, 1980, no. 5, p. 34.
12. Bulatov, V.P., Vedeneev, V.I., Kitaigorodskii, A.N., Sarkisov, O.M., Bulatov, V.P., and Vedeneev, V.I., *Izv. Akad. Nauk SSSR, Ser. Khim.*, 1975, no. 9, p. 1882.
13. Azatyan, V.V., Kalkanov, V.A., and Shavard, A.A., *React. Kinet. Catal. Lett.*, 1980, vol. 15, p. 367.
14. Nagorny, S.S., Rubtsov, N.M., Temchin, S.M., and Azatyan, V.V., *Proc. Zel'dovich Memorial*, 1994, vol. 2, p. 54.
15. Ballou, F., Lisbet, R., and Dupre, G., *Proc. 7th Int. Symp. on Loss Prevention and Safety Promotion in the Process Industies*, Taormine, 1992, p. 43.
16. Cze, C., *VLSI Technoogy*, New York: Wiley, 1981, vol. 1, p. 905.
17. Azatyan, V.V., Borodulin, R.R., Markevich, E.A., Rubtsov, N.M., and Semenov, N.N., *Izv. Akad. Nauk SSSR, Ser. Khim.*, 1976, no. 10, p. 1459.
18. Rubtsov, N.M., *Mendeleev Commun.*, 1998, p. 173.
19. Rubtsov, N.M. and Kotelkin, V.D., *Mendeleev Commun.*, 2001, p. 61.
20. Karpov, V.P., Rubtsov, N.M., Ryzhkov, O.T., Tsvetkov, G.I., and Chernysh, V.I., 2000, *Khim. Fiz.*, vol. 19, no. 8, p. 74.
21. Azatyan, V.V., Borodulin, R.R., Markevich, E.A., and Rubtsov, N.M., *Fiz. Goreniya Vzryva*, 1978, no. 14, p. 20.
22. Karpov, V.P., Rubtsov, N.M., Tsvetkov, G.I., and Chernysh, V.I., *Khim. Fiz.*, 1998, vol. 17, no. 4, p. 73.
23. Rubtsov, N.M., Ryzhkov, O.T., and Chernysh, V.I., *Kinet. Katal.*, 1995, vol. 36, no. 5, p. 645.
24. Rubtsov, N.M., Azatyan, V.V., and Borodulin, R.R., *Izv. Akad. Nauk SSSR, Ser. Khim.*, 1980, no. 29, p. 1165.
25. Azatyan, V.V., Borodulin, R.R., Markevich, E.A., Rubtsov, N.M., and Semenov, N.N., *Dokl. Akad. Nauk SSSR*, 1975, vol. 224, p. 1096.
26. Rubtsov, N.M. and Borodulin, R.R., in *Kinetika i mekhanizm fiziko-khimicheskikh reaktsii* (Kinetics and Mechanism of Physicochemical Reactions), Chernogolovka, 1981, p. 14.
27. Clark, T.C. and Clyne, M.A.A., *Trans. Faraday Soc.*, 1970, vol. 66, p. 372.

28. Azatyan, V.V., Borodulin, R.R., and Rubtsov, N.M., *Dokl. Akad. Nauk SSSR*, 1979, vol. 249, p. 1375.
29. Kaganova, Z.I. and Novozhilov, B.V., *Khim. Fiz.*, 1982, no. 1, p. 1110.
30. Clark, M.A.A. and Cruse, H.W., *J. Chem. Soc., Faraday Trans. II*, 1972, vol. 68, no. 8, p. 1281.
31. Clyne, M.A.A. and Stedman, D.H., *Trans. Faraday Soc.*, 1968, vol. 64, p. 2698.
32. Clark, T.C. and Clyne, M.A.A., *J. Chem. Soc., Trans. Faraday Soc.*, 1970, vol. 66, p. 372.
33. Apin, A.Ya., *Zh. Fiz. Khim.*, 1940, vol. 14, p. 494.
34. Posvyanskii, V.S., *Cand. Sci. (Phys.–Math.) Dissertation*, Moscow: Inst. of Chemical Physics, 1976, p. 134.
35. *Tablitsy fizicheskikh velichin* (Tables of Physical Quantities), Kikoin, I.K., Ed., Moscow: Atomizdat, 1976.
36. Rubtsov, N.M., Borodulin, R.R., and Saidkhanov, S.S., *Khim. Fiz.*, 1984, no. 3, p. 521.
37. Karpov, V.P., Chernysh, V.I., Rubtsov, N.M., and Temchin, S.M., *Archivum Combust.*, 1995, vol. 15, nos. 1–2, p. 25.

APPENDIX

At the distribution of the Y_i functions specified at the initial time moment, their further evolution is determined by system (1) with boundary conditions (2). The finite-difference approximation of system (1) on the uniform lattice of the Cartesian coordinates was used for the numeric solution. The two-step implicit scheme provided the second order of approximation (1) with respect to the spatial and time variables [16]. The results were obtained for 500 points of division over the ξ coordinate and 100 points of division over the η coordinate. The Laplacian was approximated by the "cross" scheme. The boundary conditions at the wall and in the symmetry axis of the reactor were approximated with second-order accuracy, and the partial derivatives with respect to time were approximated by one-sided differences providing first-order accuracy. Integration was performed by the explicit scheme. New values of concentrations corresponding to the occurrence of chemical reactions were simulated first, and then these values were corrected taking into account diffusion processes. The local "wave" rates $(dY_3/dt)/(dY_3/dx)$ were simulated to monitor the attainment of the numerical experiment to the "running wave" regime. The calculation process was reflected graphically on the display, which made it possible to change the simulated parameters during counting and to determine the time of its end in the conversational mode. The shape of the front of the initial component in the cross sections parallel to the reactor axis were approximated by the correlation $Y_3 = 1/2 - 1/\pi(\arctan(b_3\xi))$, and the fronts of the initial concentrations of intermediate products and temperatures in these cross-sections were specified in the form $Y_i = a_i\exp(-b_i\xi^2)$, where a_i and b_i are the scaling coefficients. For the intermediate products $a_i < 1$, and for the temperature a_4 was varied in the 200–2000 interval, which corresponded to the peak intensity of the initial pulse of a temperature of 200–2000 K. Thus, the specified initial fronts were imitated using initiation by an external source, as it is usually performed in experiments. Note that when system (1) contained the solution in the form of a running wave then it was achieved regardless of the initial conditions. Thus, the rates of the initial fronts change during integration until the achievement of the regime of propagation of all fronts Y_i with the same rate or the zero rate. For the quantitative estimation of the moment when the solution attained the running wave regime, the rates of spatial migration of points in which $Y_3 = 0.2$, 0.5, and 0.8 were calculated and displayed (see Figs. 4c, 4d). It was considered that the running wave regime is achieved when the average rate determined from these points remained unchanged at a distance of 100 characteristic sizes of the flame front. This regime is achieved rather rapidly in the middle of the flame propagation region and much more slowly at the limits of the nonthermal flame propagation. When prolonged calculations were necessary, the following procedure was used. The running wave occupied up to 50 units of the lattice. When the wave approached the left boundary of the simulated region and was completely localized in the left 100 units of the lattice (only zero values were at the right), the Y_i values from the left part of the lattice were transferred to the right part, and counting was continued. This method was quantitatively verified in [19] in comparison with simulated data from [29].